Tuned Positive Position Feedback Control of an Active Magnetic Bearings System With 16-Poles and Constant Stiffness

ALI KANDIL [ID]1 AND Y. S. HAMED [ID]2

[1]Department of Physics and Engineering Mathematics, Faculty of Electronic Engineering, Menoufia University, Menouf 32952, Egypt
[2]Department of Mathematics and Statistics, College of Science, Taif University, Taif 21944, Saudi Arabia

Corresponding author: Ali Kandil (alikandil21@yahoo.com)

ABSTRACT This paper presents a tuned positive position feedback controller (TPPF) to overcome the dual high peaks of the classical PPF. This control signal is merged with a proportional-derivative (PD) control signal to suppress the vibrations of a constant-stiffness 16-poles rotor active magnetic bearings (AMBs) system. Another benefit of the applied TPPF is turning the rotor's quasiperiodic unstable motion into a periodic stable motion by eliminating both saddle-node and Hopf points. The whole group equations of motion are derived and their approximate solutions are sought with the aid of the multiple scales method. Different response curves are plotted to clarify the difference between the rotor's vibratory behaviors before and after PPF and also with TPPF.

INDEX TERMS Tuned positive position feedback controller, proportional derivative controller, active magnetic bearings, quasiperiodic motion, saddle-node points locus, Hopf points locus.

I. INTRODUCTION

Several dynamical structures may suffer from unwanted vibrations because they can harm or even destroy the structures. Huge number of research papers focus on analyzing and controlling these vibrations via passive and/or active techniques. One of the most successful techniques in the field of active vibration control is the positive position feedback (PPF) active controller. Many researchers have devoted their entire time to improve the PPF controller performance. Shan *et al.* [1] analyzed the application of PPF control algorithm on the piezo actuators in order to mitigate the vibrations of a single-link flexible manipulator. Gospodarič *et al.* [2] dealt with the electromagnetic active damping of a clamped-cantilever lateral vibration. They produced a simulation of the control system and confirmed the results by experimental work. Liu and Hu [3] proposed a systematic approach in order to stabilize the unstable or critically stable equilibrium of linear undamped systems using position feedbacks (without and with time delays). Mahmoodi and Ahmadian [4] presented a modified PPF as an alternative to the classical PPF. They employed a first-order oscillator for damping and a second-order oscillator for suppression. Orszulik and Shan [5] developed an active control scheme for a flexible manipulator with a piezo-electric sensor/actuator pair. They combined the PPF with a recursive-least-squares adaptive parameter estimator so as to update the structure's natural frequencies online. Warminski *et al.* [6] applied different control strategies for a nonlinear flexible beam with macro fiber composite actuator. They have tried out the PPF which gave them remarkable results for suppressing the vibrations. Kandil *et al.* [7], [8] involved the time delay in the PPF to examine its effects on the stability of both an excited magnetically-levitated body and a rotating blade. Huang and Xu [9] investigated the performance of a delayed PPF on a viscoelastic isolation system with a real-power restoring force. They chose the feedback parameters by combining the desired stability conditions. Garcia-Perez *et al.* [10] proposed a multiple PPF to deal with the asymptotic trajectory tracking on a flexible-link robot which was modeled and validated via finite element methods and experimental modal analysis. Bin *et al.* [11] determined optimal parameters of PPF to be used for suppressing flexible structures vibrations based on solving the $H\infty$ synthesis problem. Hamed *et al.* [12] applied the PPF through a macro fiber composite actuator to control a rotating blade vibratory behavior. They adopted

The associate editor coordinating the review of this manuscript and approving it for publication was Guangdeng Zong [ID].

an asymptotic analysis to understand the resulting nonlinear phenomena.

Regarding the dynamical structures that may suffer from unwanted vibrations, our case of study here is a suspended rotor in an active magnetic bearings (AMBs) system. This vibratory system has been analyzed in many researches. Ji and Hansen [13], [14] investigated the nonlinear dynamical behavior of a suspended rotor via AMBs. They studied the effects of the absence and presence of time delays in the feedback control loop. Zhang and Zhan [15] utilized a perturbation method to look for the chaotic motions in a rotor-AMB system with a periodic time-varying stiffness. Ji *et al.* [16] summarized the development on the nonlinear dynamics of AMBs and its relation to the nonlinear properties and time delays. Inoue *et al.* [17] considered a vertically-supported rotor in an AMBs system, and investigated the time delay effects on the dynamical characteristics. Li *et al.* [18] applied the multiple scales method to analyze the response of dual modes of a rotor-AMBs system near the primary resonance case. Yang *et al.* [19] found that the in-unison motions did not exist for the suspended rotor in an AMBs system, while the elliptic motions were located. Wu *et al.* [20] investigated the nonlinear dynamics of a rotor-AMBs system with 16-poles and periodic time-varying stiffness near resonances. Jha and Dasgupta [21] studied the effects of an eccentric shaft-disk system with an internal damping excited by a non-ideal power source which revealed instability in high speed rotors. Sun *et al.* [22] applied a cell mapping method in order to analyze the nonlinear characteristics of an AMBs system at which the instability was due to the parameters bifurcation. Wang *et al.* [23] introduced a hybrid feedback control method to overcome the Hopf bifurcation behavior of the AMBs system. Fang *et al.* [24] explored, for worn oil-lubricated rolling bearings, the nonlinear dynamical behavior and response including the trajectory effect of the film thickness, the axis center, and the accelerated speed. Kandil *et al.* [25]–[28] studied controlling the vibrations of 8-poles and 16-poles rotor-AMBs with constant stiffness. They tried to show the effects of parameters on the solutions multiplicity and the motion asymmetry and stability. Ma *et al.* [29] investigated a 16-poles rotor-AMBs system for its stability and Shilnikov-type multipulse jumping chaotic motions. It is worthy to mention that Sun *et al.* [33]–[35] focused on modelling the maglev vehicle–guideway interaction vibration problem during operation. They discussed the control parameters effects of both fuzzy control and fuzzy adaptive tuning PID control on the vehicle–guideway coupling system. Also, they proposed an amplitude saturation controller for only saturated unidirectional attractive force as the neural network learned the control trend. To overcome some control problems, they applied a semi-supervised controller based on deep belief network algorithm where unknown external disturbances existed.

All the aforementioned researches have discussed analyzing and controlling the 4-pole, 8-pole, 16-pole rotor-AMBs systems via adjusting the system physical parameters or via different active control algorithms. All of these algorithms
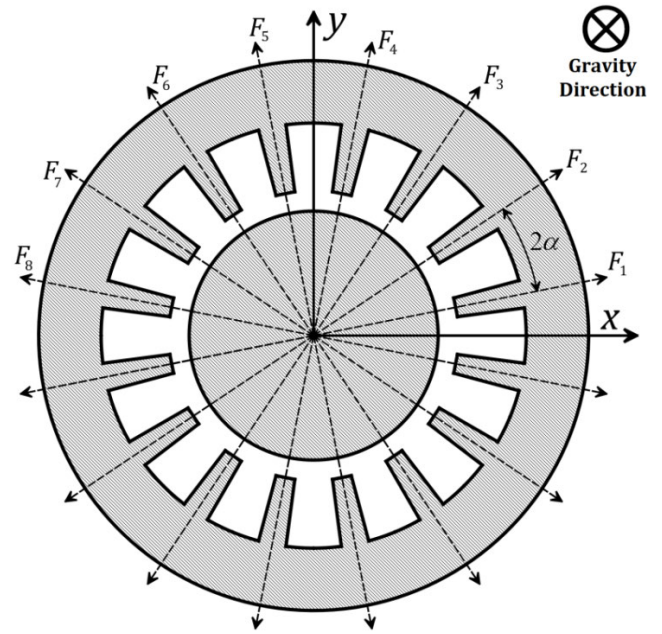

FIGURE 1. Plan view of a vertically-supported 16-pole rotor-AMB model.

were useful in reducing vibrations for only one or few operating conditions at both fixed rotor's speed and/or eccentricity. In this work, we are applying the PPF controller with the possibility of tuning it to reach the minimum vibratory levels of a rotor in an AMBs system involving 16 poles and constant stiffness. We are adapting the PPF controller in the face of sudden changes in both rotor's speed and/or eccentricity. This can be done by tuning the PPF's natural frequency ω_c to the rotor's speed Ω. The PPF control signal is merged with the original PD signal to extend the control job. Approximate solutions of the whole set are extracted via the multiple scales perturbation technique. Different response curves are plotted in order to clarify the difference between the system before and after using PPF.

II. SYSTEM MODELLING AND MULTIPLE SCALES ANALYSIS

For a vertically-supported rotor as shown in Fig. 1, its weight is not be considered. The motion of its center is governed by the following equations:

$$m\ddot{x} + \zeta\dot{x} - R_x = mE\Omega^2\cos(\Omega t) \tag{1a}$$

$$m\ddot{y} + \zeta\dot{y} - R_y = mE\Omega^2\sin(\Omega t) \tag{1b}$$

where m, E, Ω are the mass, eccentricity, and rotating angular speed of the studied rotor, respectively. ζ is an assumed small viscous damping factor. R_x and R_y are the horizontal and vertical magnetic restoring forces that will be computed later. Equation (1) is valid in case of considering the rotor as a one rigid (non-elastic) mass with two degrees of freedom.

The rotor is suspended and supported magnetically as shown by 16 uniformly-distributed poles (electromagnets) with an angle $2\alpha = \pi/8$ between each two poles. Every

opposed pair of poles produces an electromagnetic force F_n ($n = 1, \ldots, 8$) which is defined as [30]:

$$F_n = K\left[\frac{(I_0 - I_n)^2}{(\delta - w_n)^2} - \frac{(I_0 + I_n)^2}{(\delta + w_n)^2}\right] \quad (2)$$

where K is a constant depending on the poles design, I_0 is the constant initial current for magnetization, δ is the clearance fit between the stator and the rotor, I_n is the variable control current to be applied in every nth pair of poles, w_n is the radial position of the rotor's center in the nth direction. Equation (2) is already applicable to a 16-pole magnetic bearing based on Refs. [20], [26]–[30]. It is valid in case of neglecting the eddy current losses, the hysteresis and saturation of the magnetic core material, and the magnetic coupling between the poles. The currents I_n are computed due to PD control algorithm plus an additional control signal as follows

$$I_n = k_p w_n + k_d \dot{w}_n - k_1 W_n \quad (3)$$

where k_p, k_d are the PD gains, k_1 is the additional control signal gain. The quantities w_n and W_n are proposed as

$$w_n = x\cos((2n-1)\alpha) + y\sin((2n-1)\alpha) \Rightarrow \dot{w}_n$$
$$= \dot{x}\cos((2n-1)\alpha) + \dot{y}\sin((2n-1)\alpha) \quad (4a)$$
$$W_n = u\cos((2n-1)\alpha) + v\sin((2n-1)\alpha) \quad (4b)$$

where u, v are the output signals generated from two virtual oscillators (PPF oscillators) that are in the form

$$\ddot{u} + \zeta_c \dot{u} + \chi_c^2 u = k_2 x \quad (5a)$$
$$\ddot{v} + \zeta_c \dot{v} + \chi_c^2 v = k_2 y \quad (5b)$$

where ζ_c, χ_c are the damping factor and natural frequency of the proposed oscillator, k_2 is the feedback signals gain. Substituting Eqs. (3) and (4) into (2) then computing the Cartesian components of the resultant magnetic restoring forces into a third order Maclaurin expansion as

$$R_x = \sum_{n=1}^{8} F_n \cos[(2n-1)\alpha]$$
$$= \eta_1 k_d \dot{x} + \eta_2 x + \eta_3\left(x^3 + xy^2\right)$$
$$+ \eta_4 k_d\left(\dot{x}y^2 + 2xy\dot{y} + 3x^2\dot{x}\right)$$
$$+ \eta_5 k_d^2\left(x\dot{y}^2 + 2\dot{x}y \, doty + 3x\dot{x}^2\right)$$
$$- \eta_4 k_1\left(uy^2 + 2vxy + 3ux^2\right)$$
$$- 2\eta_5 k_1 k_d\left(uy\dot{y} + v\dot{x}y + vx\dot{y} + 3ux\dot{x}\right)$$
$$+ \eta_5 k_1^2\left(v^2 x + 2uvy + 3u^2 x\right) - \eta_1 k_1 u \quad (6a)$$

$$R_y = \sum_{n=1}^{8} F_n \sin[(2n-1)\alpha]$$
$$= \eta_1 k_d \dot{y} + \eta_2 y + \eta_3\left(y^3 + x^2 y\right)$$
$$+ \eta_4 k_d\left(x^2\dot{y} + 2x\dot{x}y + 3y^2\dot{y}\right)$$
$$+ \eta_5 k_d^2\left(\dot{x}^2 y + 2x\dot{x}\dot{y} + 3y\dot{y}^2\right)$$

$$- \eta_4 k_1\left(vx^2 + 2uxy + 3vy^2\right)$$
$$- 2\eta_5 k_1 k_d\left(vx\dot{x} + ux\dot{y} + u\dot{x}y + 3vy\dot{y}\right)$$
$$+ \eta_5 k_1^2\left(u^2 y + 2uvx + 3v^2 y\right) - \eta_1 k_1 v \quad (6b)$$

where

$$\eta_1 = -\frac{16KI_0}{\delta^2}$$
$$\eta_2 = \frac{16K}{\delta^3}\left[I_0^2 - k_p \delta I_0\right]$$
$$\eta_3 = \frac{12K}{\delta^5}\left[2I_0^2 - 3k_p \delta I_0 + k_p^2 \delta^2\right]$$
$$\eta_4 = \frac{4K}{\delta^4}\left[2k_p \delta - 3I_0\right]$$
$$\eta_5 = \frac{4K}{\delta^3}$$

To increase the comprehensibility, we will normalize the rotor's horizontal (x) and vertical (y) displacements by comparing them to the stator-rotor's gap δ. This can be done to the controller signals u and v too. A further simplification is reached by normalizing the time t and the rotor's speed Ω. Substituting Eqs. (6) into (1) with using $x^* = x/\delta$, $y^* = y/\delta$, $u^* = u/\delta$, $v^* = v/\delta$, $t^* = t\sqrt{KI_0^2}/\sqrt{m\delta^3}$, $\Omega^* = \Omega\sqrt{m\delta^3}/\sqrt{KI_0^2}$ in order to normalize the results and Eqs. (5). The asterisks are removed for brevity to obtain

$$\ddot{x} + \mu\dot{x} + \omega^2 x + \alpha_1\left(x^3 + xy^2\right)$$
$$+ \alpha_2\left(\dot{x}y^2 + 2xy\dot{y} + 3x^2\dot{x}\right)$$
$$+ \alpha_3\left(x\dot{y}^2 + 2\dot{x}y\dot{y} + 3x\dot{x}^2\right)$$
$$+ \beta_1\left(uy^2 + 2vxy + 3ux^2\right)$$
$$+ \beta_2\left(uy\dot{y} + v\dot{x}y + vx\dot{y} + 3ux\dot{x}\right)$$
$$+ \beta_3\left(v^2 x + 2uvy + 3u^2 x\right)$$
$$= f\Omega^2\cos(\Omega t) + 16\lambda u \quad (7a)$$
$$\ddot{y} + \mu\dot{y} + \omega^2 y + \alpha_1\left(y^3 + x^2 y\right)$$
$$+ \alpha_2\left(x^2\dot{y} + 2x\dot{x}y + 3y^2\dot{y}\right)$$
$$+ \alpha_3\left(\dot{x}^2 y + 2x\dot{x}\dot{y} + 3y\dot{y}^2\right)$$
$$+ \beta_1\left(vx^2 + 2uxy + 3vy^2\right)$$
$$+ \beta_2\left(vx\dot{x} + ux\dot{y} + u\dot{x}y + 3vy\dot{y}\right)$$
$$+ \beta_3\left(u^2 y + 2uvx + 3v^2 y\right)$$
$$= f\Omega^2\sin(\Omega t) + 16\lambda v \quad (7b)$$
$$\ddot{u} + \mu_c\dot{u} + \omega_c^2 u = \lambda x \quad (7c)$$
$$\ddot{v} + \mu_c\dot{v} + \omega_c^2 v = \lambda y \quad (7d)$$

where

$$p = \frac{\delta k_p}{I_0} \quad d = \frac{k_d\sqrt{K}}{\sqrt{m\delta}} \quad c = \frac{\zeta\delta\sqrt{\delta}}{I_0\sqrt{mK}} \quad f = \frac{E}{\delta}$$
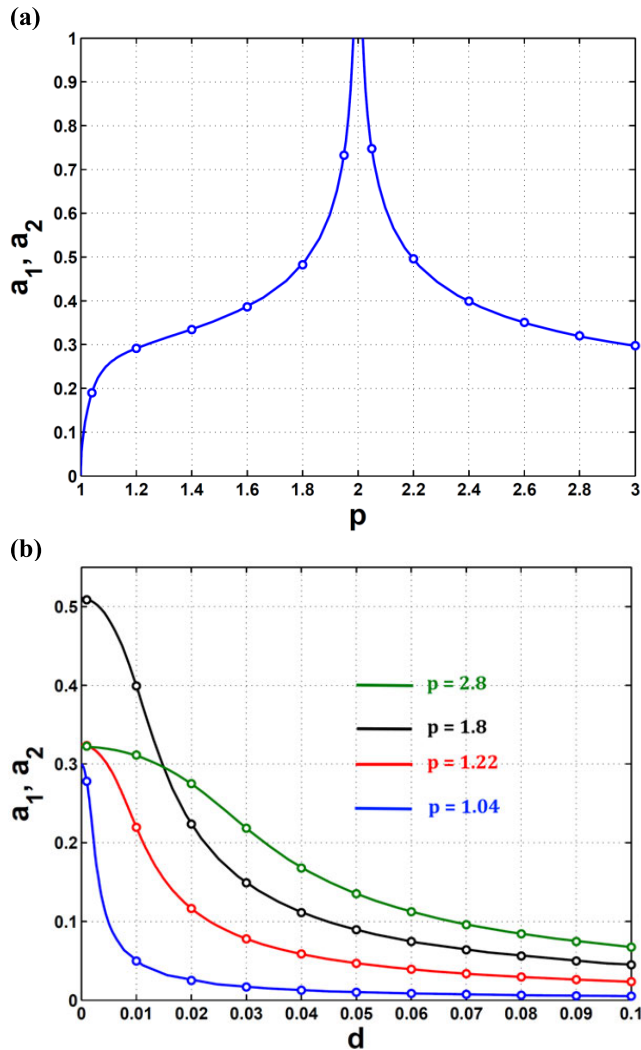
(a)

(b)

FIGURE 2. Effects of varying the parameters p and d on the rotor's vibratory amplitudes at $\sigma = 0$: (a) varying p, (b) varying d.

$$\lambda = \frac{\delta k_1}{I_0} = \frac{k_2 m \delta^3}{K I_0^2} \quad \mu_c = \frac{\zeta_c \delta \sqrt{m\delta}}{I_0 \sqrt{K}}$$

$$\omega_c^2 = \frac{\chi_c^2 m \delta^3}{K I_0^2} \quad \mu = c + 16d$$

$$\omega^2 = 16(p-1) \quad \alpha_1 = -12(p-1)(p-2)$$

$$\alpha_2 = -4d(2p-3) \quad \alpha_3 = -4d^2$$

$$\beta_1 = 4\lambda(2p-3) \quad \beta_2 = 8\lambda d \quad \beta_3 = -4\lambda$$

Equations (7) represent a constant-stiffness coefficients model due to the time-invariant stiffness coefficients α_1, α_2, α_3, β_1, β_2, β_3. These coefficients depend on p, d, λ that are constant during every individual rotor's operation. This is unlike some previous works of time-varying stiffness where they treated p, d as time-varying periodic coefficients during every individual rotor's operation. With the benefit of the multiple scales method [31], first-order approximate solutions of Eqs. (7) are generated when $\Omega \approx \omega$ and $\omega_c \approx \omega$. We have determined the equations governing the amplitudes

(a_i) and phases (ϕ_i) modulations of the rotor's vibrations and the controller. The result is,

$$
\begin{aligned}
\dot{a}_1 = &-\frac{\mu}{2}a_1 - \frac{\alpha_1 + \alpha_3 \omega^2}{8\omega}a_1 a_2^2 \sin(2\phi_1 - 2\phi_2) \\
&- \frac{\alpha_2}{8}a_1 a_2^2 \cos(2\phi_1 - 2\phi_2) - \frac{3\beta_3}{8\omega}a_1 a_3^2 \sin(2\phi_1 - 2\phi_3) \\
&- \frac{\beta_3}{8\omega}a_1 a_4^2 \sin(2\phi_1 - 2\phi_4) - \frac{3\beta_2}{8}a_1^2 a_3 \cos(\phi_1 - \phi_3) \\
&+ \left[-\frac{3\beta_1}{8\omega}a_1^2 - \frac{\beta_1}{4\omega}a_2^2 + \frac{8\lambda}{\omega}\right]a_3 \sin(\phi_1 - \phi_3) \\
&- \frac{\beta_1}{4\omega}a_1 a_2 a_4 \sin(2\phi_1 - \phi_2 - \phi_4) \\
&- \frac{\beta_1}{8\omega}a_2^2 a_3 \sin(\phi_1 - 2\phi_2 + \phi_3) \\
&- \frac{\beta_2}{8}a_2^2 a_3 \cos(\phi_1 - 2\phi_2 + \phi_3) \\
&- \frac{\beta_3}{4\omega}a_2 a_3 a_4 [\sin(\phi_1 - \phi_2 - \phi_3 + \phi_4) \\
&+ \sin(\phi_1 - \phi_2 + \phi_3 - \phi_4) + \sin(\phi_1 + \phi_2 - \phi_3 - \phi_4)] \\
&- \frac{\beta_2}{4}a_1 a_2 a_4 \cos(\phi_2 - \phi_4) - \frac{3\alpha_2}{8}a_1^3 - \frac{\alpha_2}{4}a_1 a_2^2 \\
&+ \frac{f\Omega^2}{2\omega}\sin(\phi_1) \quad\quad\quad (8a)
\end{aligned}
$$

$$
\begin{aligned}
\dot{\phi}_1 = &\ \sigma - \frac{\alpha_1 + \alpha_3 \omega^2}{8\omega}a_2^2 \cos(2\phi_1 - 2\phi_2) \\
&+ \frac{\alpha_2}{8}a_2^2 \sin(2\phi_1 - 2\phi_2) - \frac{3\beta_3}{8\omega}a_3^2 \cos(2\phi_1 - 2\phi_3) \\
&- \frac{\beta_3}{8\omega}a_4^2 \cos(2\phi_1 - 2\phi_4) \\
&+ \left[-\frac{9\beta_1}{8\omega}a_1 - \frac{\beta_1}{4\omega}\frac{a_2^2}{a_1} + \frac{8\lambda}{\omega a_1}\right]a_3 \cos(\phi_1 - \phi_3) \\
&- \frac{3\beta_2}{8}a_1 a_3 \sin(\phi_1 - \phi_3) - \frac{\beta_1}{4\omega}a_2 a_4 \cos(2\phi_1 - \phi_2 - \phi_4) \\
&- \frac{\beta_1}{8\omega a_1}a_2^2 a_3 \cos(\phi_1 - 2\phi_2 + \phi_3) \\
&+ \frac{\beta_2}{8a_1}a_2^2 a_3 \sin(\phi_1 - 2\phi_2 + \phi_3) \\
&- \frac{\beta_3}{4\omega a_1}a_2 a_3 a_4 [\cos(\phi_1 - \phi_2 - \phi_3 + \phi_4) \\
&+ \cos(\phi_1 - \phi_2 + \phi_3 - \phi_4) + \cos(\phi_1 + \phi_2 - \phi_3 - \phi_4)] \\
&- \frac{\beta_2}{4}a_2 a_4 \sin(\phi_2 - \phi_4) - \frac{\beta_1}{2\omega}a_2 a_4 \cos(\phi_2 - \phi_4) \\
&- \frac{3\alpha_1 + 3\alpha_3 \omega^2}{8\omega}a_1^2 - \frac{\alpha_1 + \alpha_3 \omega^2}{4\omega}a_2^2 - \frac{3\beta_3}{4\omega}a_3^2 - \frac{\beta_3}{4\omega}a_4^2 \\
&+ \frac{f\Omega^2}{2\omega}\frac{\cos(\phi_1)}{a_1} \quad\quad\quad (8b)
\end{aligned}
$$

$$
\begin{aligned}
\dot{a}_2 = &-\frac{\mu}{2}a_2 + \frac{\alpha_1 + \alpha_3 \omega^2}{8\omega}a_1^2 a_2 \sin(2\phi_1 - 2\phi_2) \\
&- \frac{\alpha_2}{8}a_1^2 a_2 \cos(2\phi_1 - 2\phi_2) - \frac{3\beta_3}{8\omega}a_2 a_4^2 \sin(2\phi_2 - 2\phi_4) \\
&- \frac{\beta_3}{8\omega}a_2 a_3^2 \sin(2\phi_2 - 2\phi_3)
\end{aligned}
$$
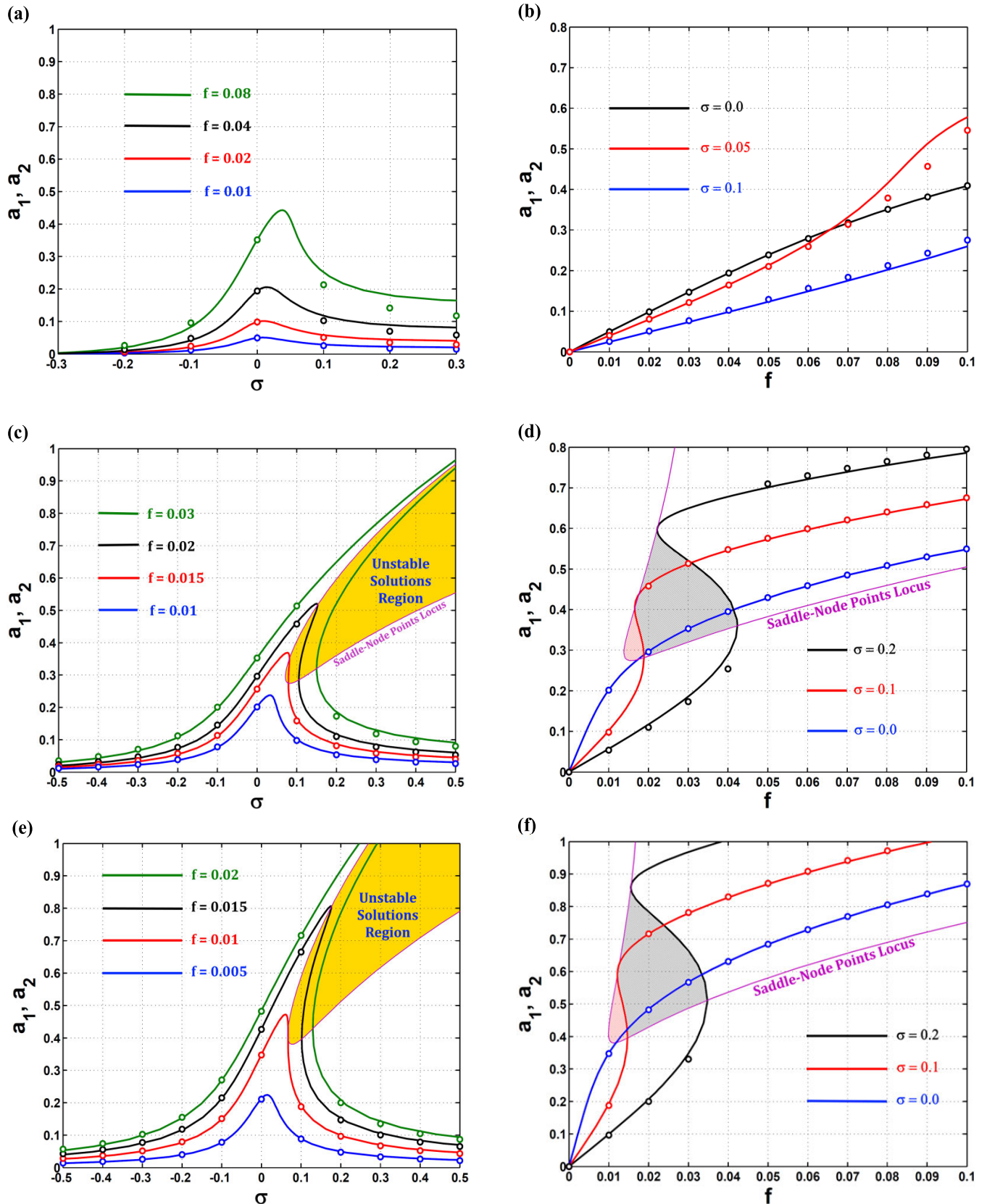
FIGURE 3. Effects of varying the rotor's speed Ω ($\sigma = \Omega - \omega$) and eccentricity f on its vibratory amplitudes at: (a, b) p = 1.04, (c, d) p = 1.22, (e, f) p = 1.8, (g, h) p = 2.8.
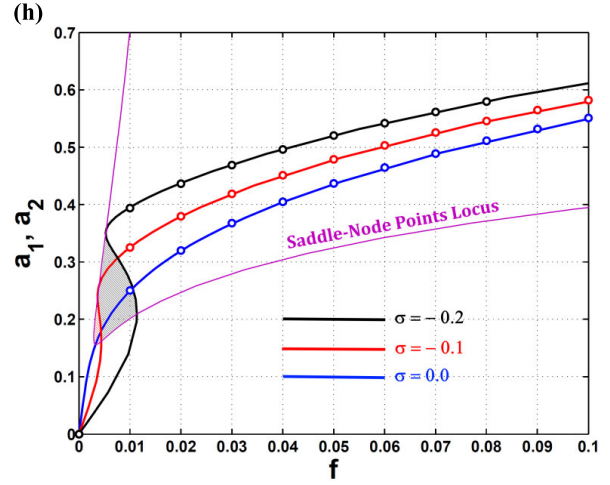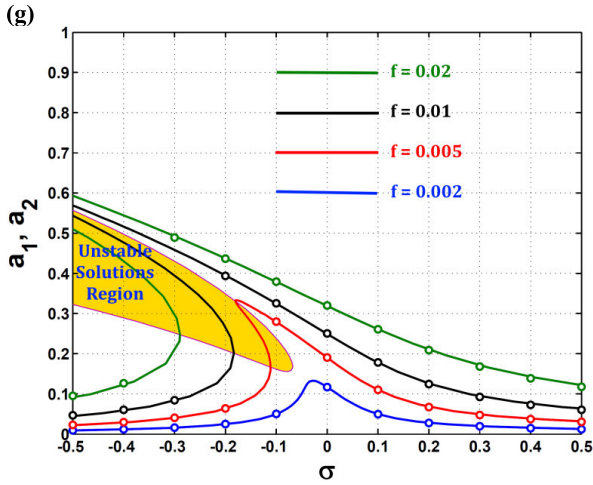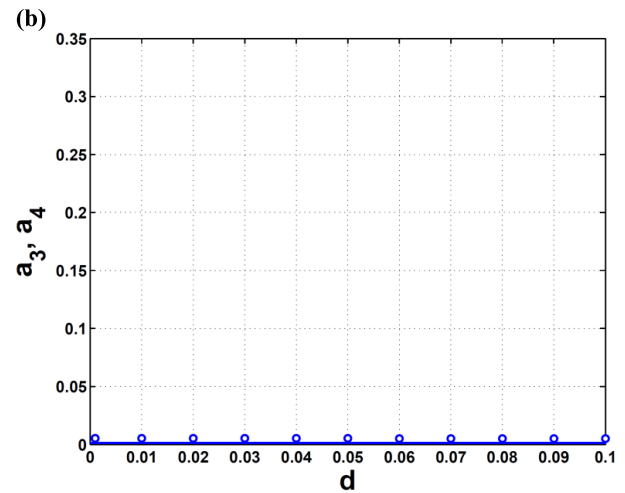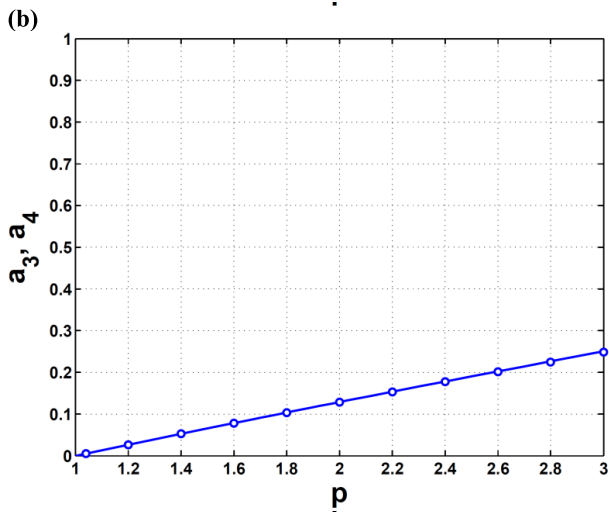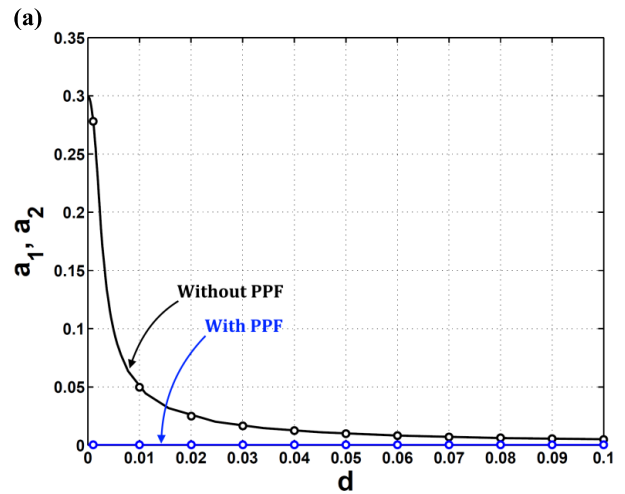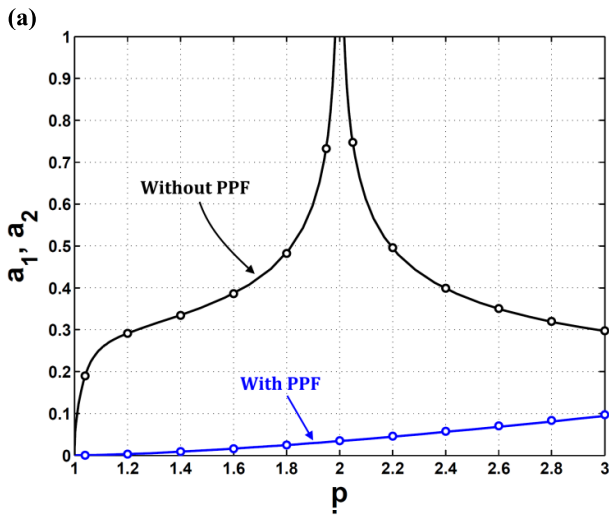
FIGURE 3. *(Continued.)* Effects of varying the rotor's speed Ω ($\sigma = \Omega - \omega$) and eccentricity f on its vibratory amplitudes at: (a, b) p = 1.04, (c, d) p = 1.22, (e, f) p = 1.8, (g, h) p = 2.8.

FIGURE 4. Effects of varying the parameter p on the (a) rotor and (b) controller amplitudes at $\sigma = 0$, and $\lambda = 0.15$.

FIGURE 5. Effects of varying the parameter d on the (a) rotor and (b) controller amplitudes at $\sigma = \sigma_c = 0$, p = 1.04, and $\lambda = 0.15$.

$$+ \left[-\frac{3\beta_1}{8\omega} a_2^2 - \frac{\beta_1}{4\omega} a_1^2 + \frac{8\lambda}{\omega} \right] a_4 \sin(\phi_2 - \phi_4)$$

$$- \frac{3\beta_2}{8} a_2^2 a_4 \cos(\phi_2 - \phi_4)$$
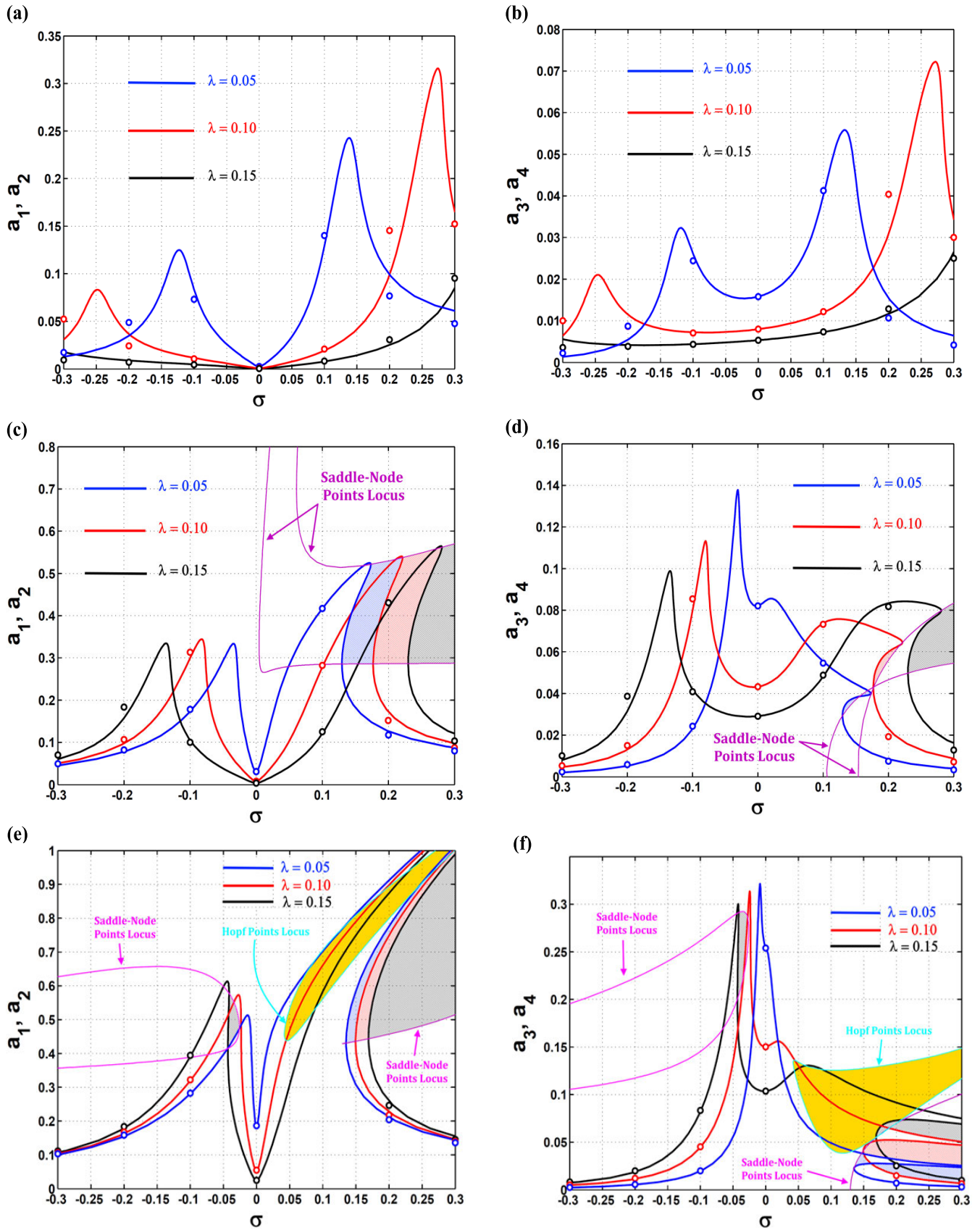$$+ \frac{\beta_1}{4\omega} a_1 a_2 a_3 \sin(\phi_1 - 2\phi_2 + \phi_3)$$

FIGURE 6. Effects of varying λ on the amplitudes-speed curves at: (a, b) p = 1.04, (c, d) p = 1.22, (e, f) p = 1.8, (g, h) p = 2.8.

(g)

(h)
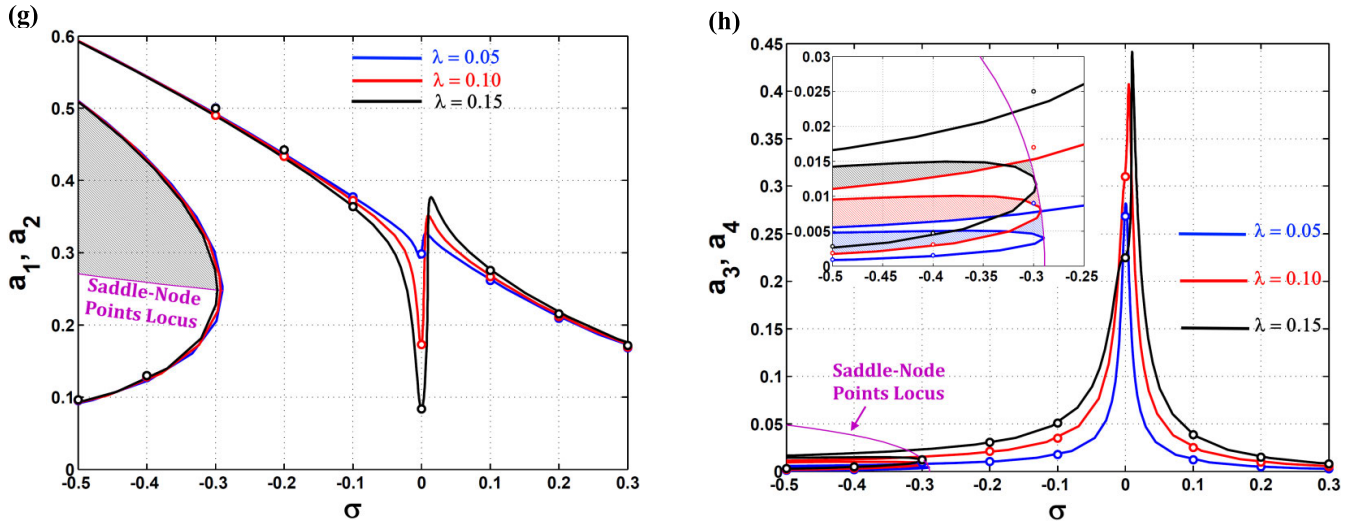

FIGURE 6. *(Continued.)* Effects of varying λ on the amplitudes-speed curves at: (a, b) p = 1.04, (c, d) p = 1.22, (e, f) p = 1.8, (g, h) p = 2.8.

$$+\frac{\beta_1}{8\omega}a_1^2a_4\sin(2\phi_1-\phi_2-\phi_4)$$

$$-\frac{\beta_2}{8}a_1^2a_4\cos(2\phi_1-\phi_2-\phi_4)$$

$$+\frac{\beta_3}{4\omega}a_1a_3a_4\left[\sin(\phi_1-\phi_2-\phi_3+\phi_4)\right.$$
$$+\sin(\phi_1-\phi_2+\phi_3-\phi_4)$$
$$\left.-\sin(\phi_1+\phi_2-\phi_3-\phi_4)\right]-\frac{\beta_2}{4}a_1a_2a_3\cos(\phi_1-\phi_3)$$

$$-\frac{3\alpha_2}{8}a_2^3-\frac{\alpha_2}{4}a_1^2a_2-\frac{f\Omega^2}{2\omega}\cos(\phi_2) \quad (8c)$$

$$\dot{\phi}_2=\sigma-\frac{\alpha_1+\alpha_3\omega^2}{8\omega}a_1^2\cos(2\phi_1-2\phi_2)$$

$$-\frac{\alpha_2}{8}a_1^2\sin(2\phi_1-2\phi_2)-\frac{3\beta_3}{8\omega}a_4^2\cos(2\phi_2-2\phi_4)$$

$$-\frac{\beta_3}{8\omega}a_3^2\cos(2\phi_2-2\phi_3)$$

$$+\left[-\frac{9\beta_1}{8\omega}a_2-\frac{\beta_1}{4\omega}\frac{a_1^2}{a_2}+\frac{8\lambda}{\omega a_2}\right]a_4\cos(\phi_2-\phi_4)$$

$$-\frac{3\beta_2}{8}a_2a_4\sin(\phi_2-\phi_4)-\frac{\beta_1}{4\omega}a_1a_3\cos(\phi_1-2\phi_2+\phi_3)$$

$$-\frac{\beta_1}{8\omega a_2}a_1^2a_4\cos(2\phi_1-\phi_2-\phi_4)$$

$$-\frac{\beta_2}{8a_2}a_1^2a_4\sin(2\phi_1-\phi_2-\phi_4)-\frac{\beta_3}{4\omega a_2}a_1a_3a_4$$
$$\times\left[\cos(\phi_1-\phi_2-\phi_3+\phi_4)+\cos(\phi_1-\phi_2+\phi_3-\phi_4)\right.$$
$$\left.+\cos(\phi_1+\phi_2-\phi_3-\phi_4)\right]-\frac{\beta_2}{4}a_1a_3\sin(\phi_1-\phi_3)$$

$$-\frac{\beta_1}{2\omega}a_1a_3\cos(\phi_1-\phi_3)-\frac{3\alpha_1+3\alpha_3\omega^2}{8\omega}a_2^2$$

$$-\frac{\alpha_1+\alpha_3\omega^2}{4\omega}a_1^2-\frac{3\beta_3}{4\omega}a_4^2-\frac{\beta_3}{4\omega}a_3^2$$

$$+\frac{f\Omega^2}{2\omega}\frac{\sin(\phi_2)}{a_2} \quad (8d)$$

$$\dot{a}_3=-\frac{\mu_c}{2}a_3-\frac{\lambda}{2\omega_c}a_1\sin(\phi_1-\phi_3) \quad (8e)$$

$$\dot{\phi}_3=\sigma-\sigma_c+\frac{\lambda}{2\omega_c a_3}a_1\cos(\phi_1-\phi_3) \quad (8f)$$

$$\dot{a}_4=-\frac{\mu_c}{2}a_4-\frac{\lambda}{2\omega_c}a_2\sin(\phi_2-\phi_4) \quad (8g)$$

$$\dot{\phi}_4=\sigma-\sigma_c+\frac{\lambda}{2\omega_c a_4}a_2\cos(\phi_2-\phi_4) \quad (8h)$$

where $\sigma=\Omega-\omega$ and $\sigma_c=\omega_c-\omega$. The fixed points of the equations above are tested for stability via the well-known Hartman-Grobman theorem [32].

III. SYSTEM BEHAVIOR IN RELATION TO PPF

In this section, the AMB system behavior is discussed for two cases. The first one is without applying the PPF controller i.e. $\lambda=0$, while the other one is with applying this controller i.e. $\lambda\neq 0$. The adopted values of the whole group are as follows: $p=1.04$, $d=0.005$, $c=0.001$, $f=0.02$, $\lambda=0.15$, $\mu_c=0.01$, $\sigma_c=0$. The rotor's vibrational amplitudes are denoted by a_1 for horizontal vibration and a_2 for vertical vibration. As we can see from Eq. (8), the quantities a_1 and a_2 are mathematical symmetrical. Hence, we combine them in the same figure to ease the readability for the reader. Figure 2 shows the effect of varying the parameters p and d on the rotor's vibrational amplitudes when $\Omega=\omega$ ($\sigma=0$) and $\lambda=0$. In Fig. 2a, it can be noticed that p should be more than 1 because $\omega=4\sqrt{p-1}$ for a reasonable rotor operation. In the range $1<p<2$, the nonlinear parameter $\alpha_1=-12(p-1)(p-2)$ is positive denoting a hardening effect. This hardening effect decays as $p\to 2$ ($\alpha_1\to 0$) which makes the rotor's vibrational amplitudes $a_{1,2}$ increase at $\sigma=0$. At $p=2$ ($\alpha_1=0$), there is no hardening effect where the response is at its peak and the
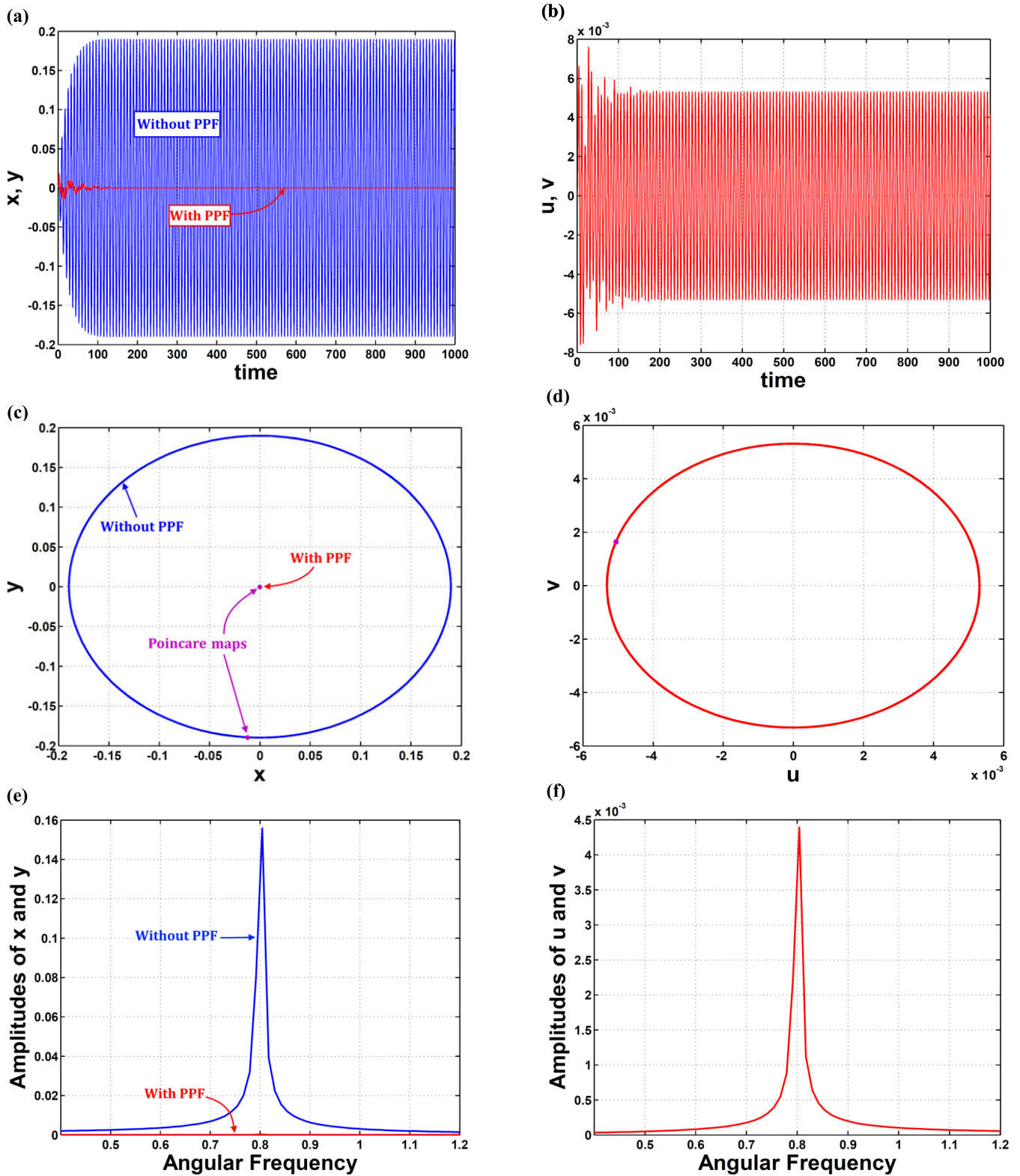
FIGURE 7. Numerical simulations of the rotor's and controller's vibratory behavior at p = 1.04, $\sigma = \sigma_c = 0$, f = 0.02, and $\lambda = 0.15$: (a, b) time responses, (c, d) orbit and Poincare maps, (e, f) amplitude spectra.

amplitudes are greater than 1 (theoretically) which means that the rotor impacts with the pole legs (practically). Moreover

for $p > 2$ ($\alpha_1 < 0$), the hardening effect is transformed into softening effect where the amplitudes begin to decrease as p
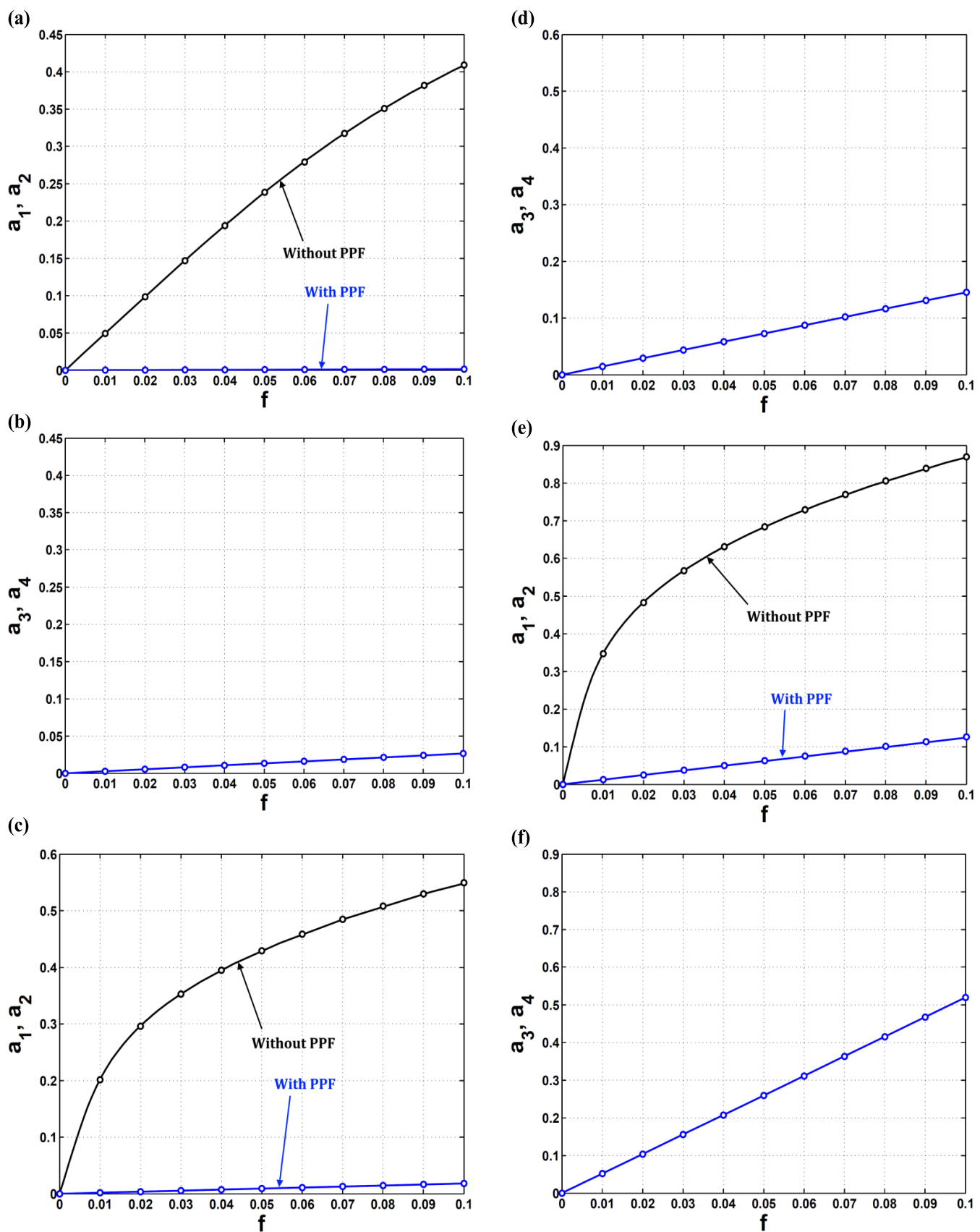
FIGURE 8. Effects of applying PPF on the rotor's and controller's amplitudes versus eccentricity f at $\sigma = \sigma_c = 0$ and $\lambda = 0.15$: (a, b) p = 1.04, (c, d) p = 1.22, (e, f) p = 1.8, (g, h) p = 2.8.
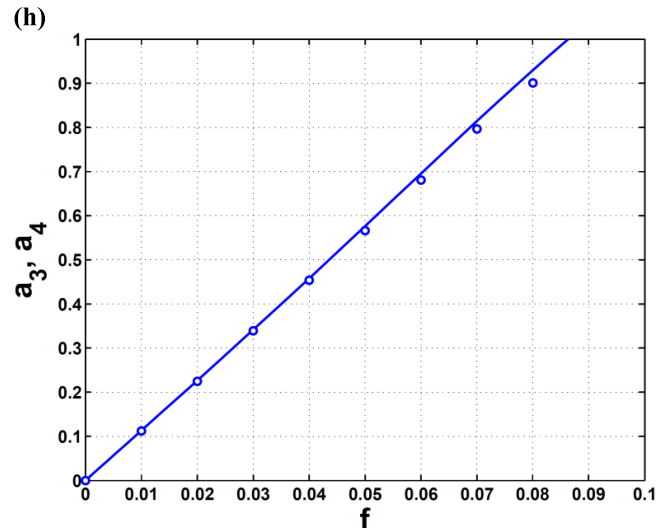
(g)

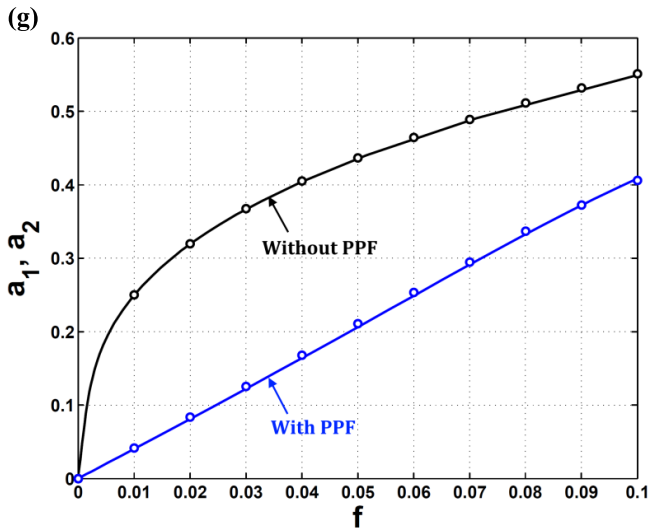**(h)**

FIGURE 8. *(Continued.)* **Effects of applying PPF on the rotor's and controller's amplitudes versus eccentricity f at** $\sigma = \sigma_c = 0$ **and** $\lambda = 0.15$: **(a, b) p = 1.04, (c, d) p = 1.22, (e, f) p = 1.8, (g, h) p = 2.8.**
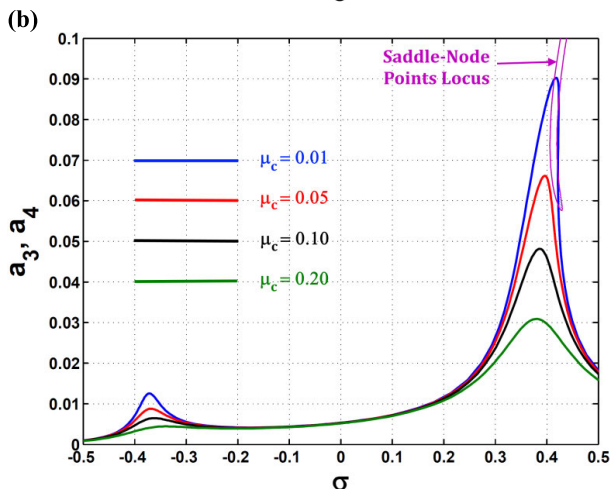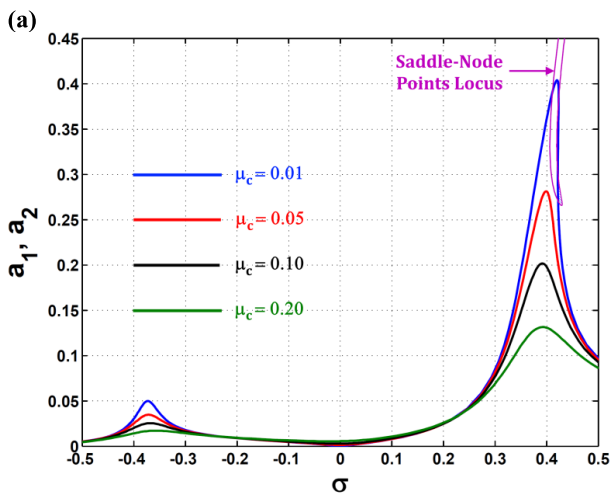
(a)

(b)

FIGURE 9. **Influence of the PPF damping** μ_c **on the undesired high peaks at f = 0.02, $\lambda = 0.15$: (a) rotor, (b) PPF.**
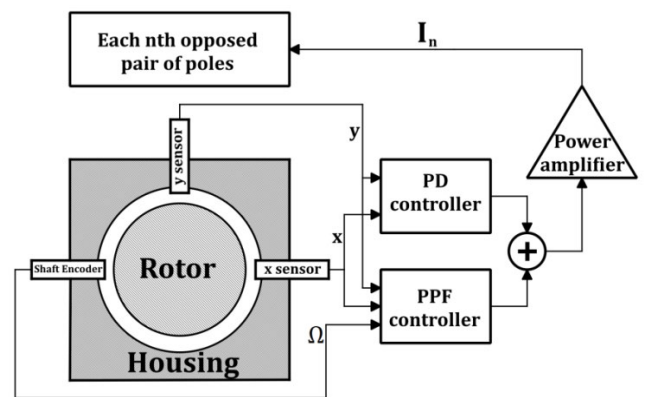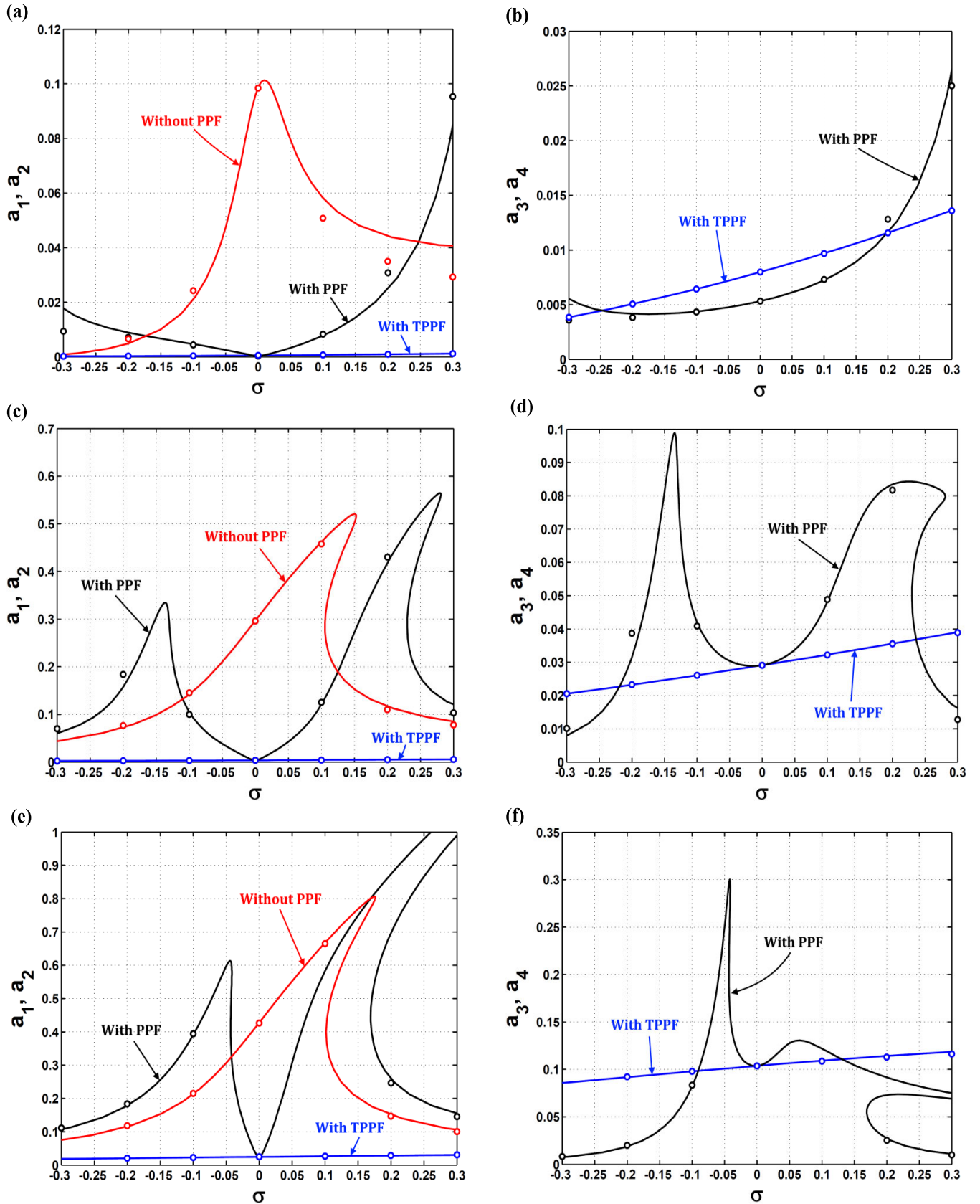
FIGURE 10. **Block diagram of TPPF control process.**

done several numerical simulation trials with different values of p. We found that $p = 1.04$ is the lower value of the p-range at which the rotor has exhibited a bounded response. For values less than 1.04, the rotor has started to exhibit an unbounded response. Hence, we adopted $p = 1.04$ as the lower value of p. On the other hand in Fig. 2b, it is clear that increasing the parameter d enhances the damping influence on the amplitudes at different values of p. The plotted circles with each curve represent numerical simulation of the rotor's equilibrium amplitudes indicating a good agreement with the analytical solid curves.

Based on Fig. 2, we are investigating the effects of varying the rotor's speed Ω and eccentricity f on its amplitudes at different values of p as shown in Fig. 3. In Figs. 3a and 3b where $p = 1.04$, the rotor's vibratory amplitudes respond linearly with both σ (at several f) and f (at several σ). In Fig. 3c where $p = 1.22$, the saddle-node bifurcation points locus appears (purple branch) and intersects with the response curves at saddle-node bifurcation points. It surrounds the whole unstable branches at different f. In Fig. 3d, this

increases. We are looking on this curve for a point where the vibrations are small enough for a safer operation. We have

FIGURE 11. Comparison between the performances of pre-PPF, PPF, and TPPF at f = 0.02 and λ = 0.15: (a, b) p = 1.04, (c, d) p = 1.22, (e, f) p = 1.8, (g, h) p = 2.8.

(g)

(h)

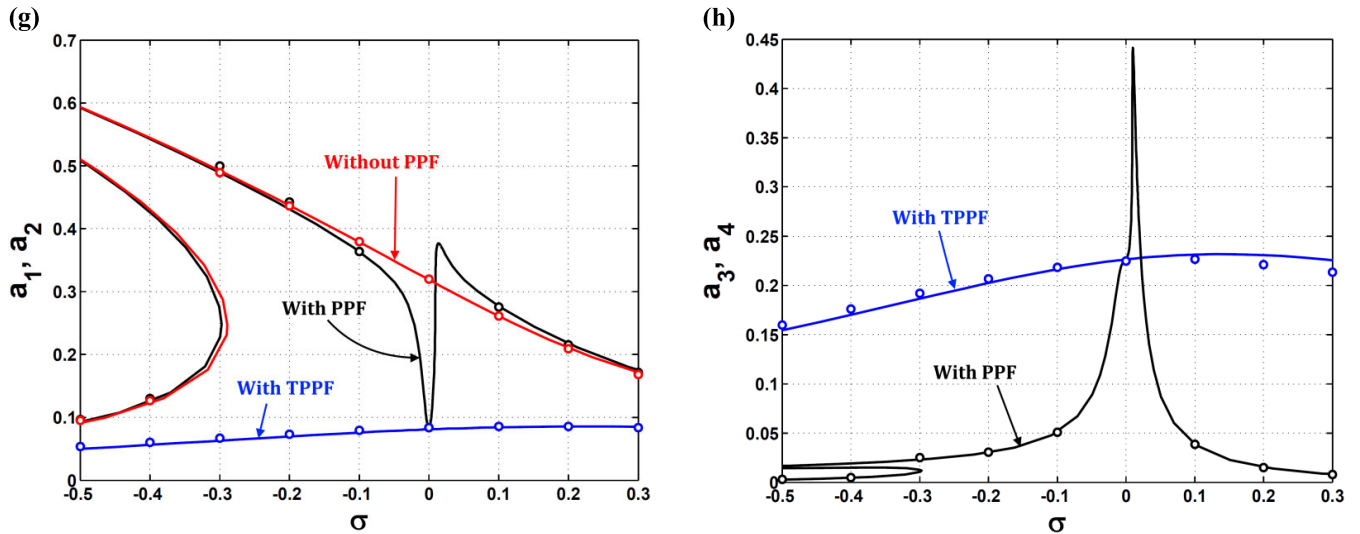**FIGURE 11.** *(Continued.)* Comparison between the performances of pre-PPF, PPF, and TPPF at f = 0.02 and λ = 0.15: (a, b) p = 1.04, (c, d) p = 1.22, (e, f) p = 1.8, (g, h) p = 2.8.

(a)

(b)

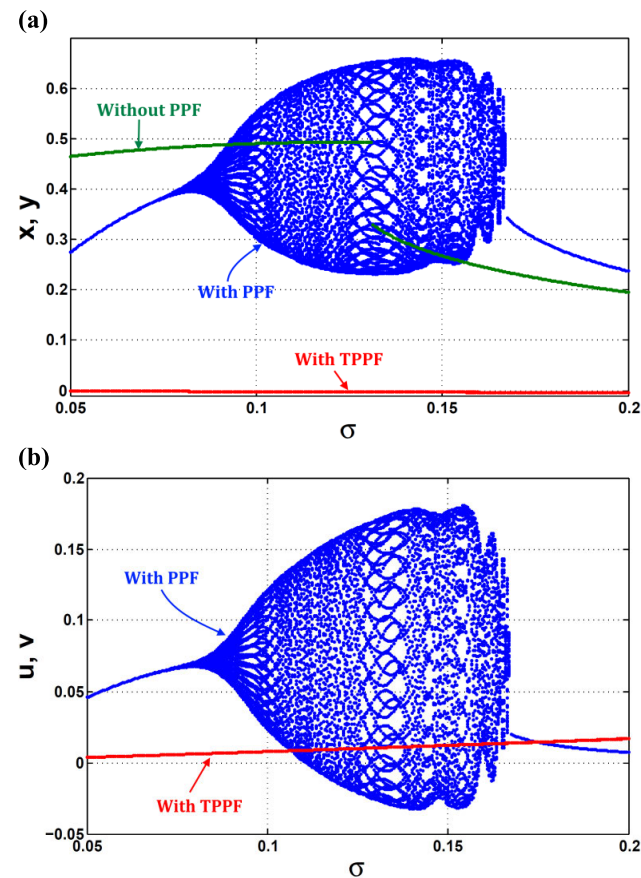**FIGURE 12.** Bifurcation diagrams of the (a) rotor's and (b) controller's vibrations versus σ without PPF, with PPF, and with TPPF at f = 0.02, p = 1.8.

locus (purple branch) intersects with the response curves at saddle-node bifurcation points without surrounding the whole unstable branches at different σ. The unstable branches here lie between the intersection points of the response curves and the locus. As the eccentricity f increases, the curves

bend to the right gradually denoting a hardening case and jump phenomena because of the positivity of α_1. Once the parameter p increases to 1.8 in Figs. 3e and 3f, the amplitudes are raised much more leading to the possibility of impacting with the pole legs (in case of $a_{1,2} \geq 1$). Figures 3g and 3h have been plotted at p = 2.8 where α_1 is negative which makes the curves bend to the left denoting a softening case as well as jump phenomena.

In case of applying the PPF controller ($\lambda \neq 0$), we are discussing its effect on the variations of p, d, σ, f with the rotor's vibrational amplitudes $a_{1,2}$. Figure 4 shows the difference between the absence and presence of the PPF controller on varying the parameter p at $\sigma = 0$ and $\lambda = 0.15$. It seems that the PPF controller dominates the rotor's vibrations in the studied range $1 < p < 3$ even at p = 2 where the rotor cannot impact with the pole legs anymore. The switching between hardening and softening effects at $\sigma = 0$ is no longer existent to be an advantage of the PPF control. Also in Fig. 5, the effect of PPF is clear in reducing the vibrations to minimum levels (almost zero) all over the studied range $0 < d < 0.1$.

As discussed in Fig. 3, Fig. 6 shows the application of PPF controller on the rotor's amplitudes versus its speed at different values of the PPF gain λ. From Eqs. (8e-h), the parameter λ can increase the PPF's steady-state amplitudes where this can widen the range of rotor's small amplitudes. It is clear from the figure that adjusting the value of λ controls the bandwidth of low amplitudes around the point $\sigma = 0$ and between the two undesired high peaks. Figures 6a and 6b show a linear form of the curves without any bifurcations or jump phenomena at p = 1.04. Also, the point $\sigma = 0$ is the minimum amplitude point where it is desired to keep the rotor in its neighborhood. At p = 1.22 in Figs. 6c and 6d, the right peaks of the response curves are intersecting with the saddle-node points locus leading to multiple solutions and jump phenomena. In Figs. 6e and 6f at p = 1.8, the saddle-node points locus intersects also
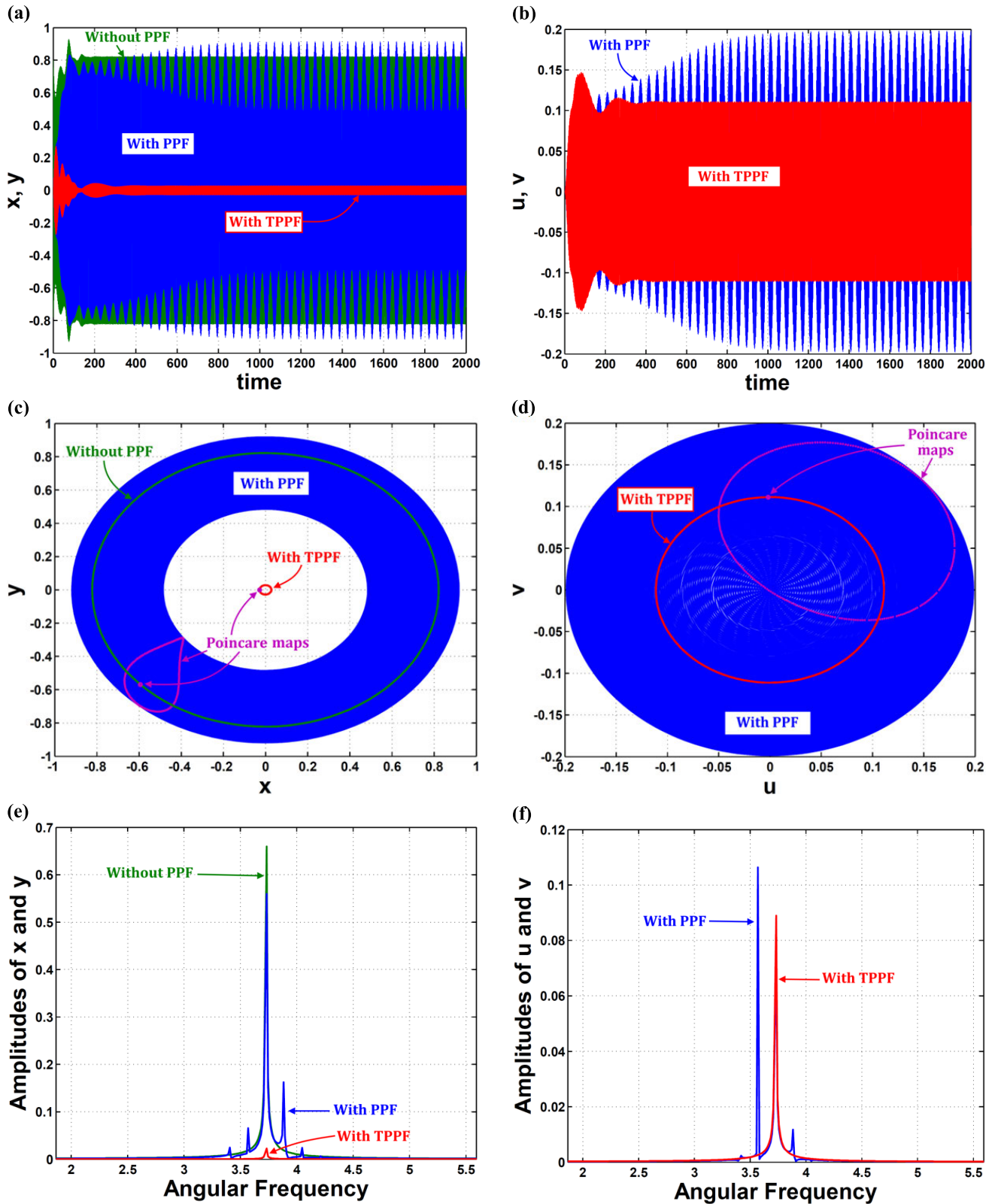
FIGURE 13. Numerical simulations of the rotor's and controller's vibratory behavior at p = 1.8, σ = 0.15, f = 0.02: (a, b) time responses, (c, d) orbit and Poincare maps, (e, f) amplitude spectra.

the left peaks of the response curves at which the issue of jump phenomena exists at both of the high peaks. Another issue is the existence of Hopf points locus which intersects

the response curves exhibiting unstable behaviors for the rotor and controller as we will treat later. Figures 6g and 6h show the response curves at $p = 2.8$ where the hardening

effect turns to softening effect because of the sign change of the parameter α_1. Figure 7 clarifies the difference before and after using PPF by supporting the discussion with time responses, orbit and Poincare maps, and amplitude spectra at $p = 1.04$ and $\sigma = \sigma_c = 0$. These plots tell us about the periodic behavior of the rotor's motion before and after using PPF at the mentioned parameters values. Also, they explain the exposition of the PPF principle based on Eqs. (8). If $\sigma = \sigma_c$ in Eqs. (8f) and (8h), the steady-state PPF's amplitudes ($a_3 \& a_4$) will have their minimum values and so the rotor's steady-state vibrational amplitudes ($a_1 \& a_2$). Since σ_c is kept constant at 0, the amplitudes increase gradually once $\sigma - \sigma_c$ increases. Later, we are going to treat this issue.

Figure 8 shows the rotor's amplitudes versus its eccentricity f at $\lambda = 0.15$, $\sigma = \sigma_c = 0$, and different values of p. In the whole figure, we can see the difference between using PPF or not. The PPF controller mitigates the rotor's vibrations efficiently regardless of its eccentricity f in Figs. 8a and 8b at $p = 1.04$. At $p = 1.22$ in Figs. 8c and 8d, the vibrations amplitudes increase slightly with f. As p increases in Figs. 8e to 8h, the rate of vibrations increases proportionally with f and this guides us to use lower values of p.

There is a way to suppress the undesired peaks by increasing the PPF damping μ_c as shown in Fig. 9. The two undesired peaks can be suppressed by raising μ_c which adds to the damping of the whole system as depicted. Another advantage, besides suppressing the peaks, is to avoid the intersection with the saddle-node points locus in order to make the rotor safe from sudden jumps (jump phenomena).

As mentioned above that if $\sigma = \sigma_c = 0$, the rotor exhibits its minimum vibratory behavior. Due to Refs. [7], [8], [12], [25], this called perfect tuning mechanism which guarantees the minimum vibratory behavior while using PPF if and only if $\sigma = \sigma_c$, or in other words, in case of $\Omega = \omega_c$. This can be done by measuring the rotor's speed Ω via a shaft encoder then providing the PPF control unit with this value to tune its natural frequency ω_c with the measured Ω. We have named the new approach a tuned PPF (TPPF). This is illustrated in Fig. 10. Figure 11 assures, with comparison, that the tuned PPF (TPPF) is the best controller to deliver minimum vibratory amplitudes in a wide range of rotor's speeds Ω at different studied values of p. Moreover, Figs. 12 and 13 show the bifurcation diagrams, time responses, orbit and Poincare maps, and amplitudes spectra for three cases of the rotor's vibrations without PPF, with PPF, and with TPPF. As can be seen in the bifurcation diagram of Fig. 12, the rotor exhibits a periodic response without PPF which appears as a single branch across different values of σ. With PPF, the response is periodic except for $0.08 \leq \sigma \leq 0.165$ where the response is either quasiperiodic (multiple branches) or sometimes chaotic (scattered dots). With TPPF, the response reverts back to its periodicity (single branch). Figure 13 assures the importance of TPPF, rather than PPF, for turning the rotor's quasiperiodic unstable motion into a periodic stable motion.

IV. CONCLUSION

This work explored the application of the PPF controller with the possibility of tuning it to reach the minimum vibratory levels of a rotor in an AMBs system involving 16 poles and constant stiffness. The PPF control signal has been merged with the original PD signal to extend the control job. Approximate solutions of the whole set were sought via the multiple scales method. Different response curves were plotted in order to clarify the difference between the system before and after PPF and also with TPPF. We can summarize some notes as follows:

- The optimum value for p was chosen to be 1.04 in order to reach small rotor vibrations.
- After applying PPF ($\lambda \neq 0$), it has dominated the rotor's vibrations in the studied range $1 < p < 3$ even at $p = 2$ where the rotor could not impact the pole legs anymore.
- Adjusting the PPF gain λ controlled the bandwidth of low amplitudes around the point $\sigma = 0$ lying between two undesired high peaks.
- The PPF's damping μ_c could be increased to suppress its undesired peaks.
- Tuned PPF could be applied if and only if $\Omega = \omega_c$ where it could be done by measuring the rotor's speed Ω and tuning it with PPF's natural frequency ω_c.
- The extreme importance of TPPF was in turning the rotor's quasiperiodic unstable motion into a periodic stable motion.
- Another importance of TPPF was suppressing the dual high peaks of the classical PPF controller.
- The only obstacle of applying TPPF was the delay in acquiring the rotor's speed Ω from the shaft encoder which made TPPF unable to do its job.

CONFLICTS OF INTEREST

The authors declare that there are no conflicts of interest associated with this publication.

REFERENCES

[1] J. Shan, H.-T. Liu, and D. Sun, "Slewing and vibration control of a single-link flexible manipulator by positive position feedback (PPF)," *Mechatronics*, vol. 15, no. 4, pp. 487–503, May 2005, doi: 10.1016/j.mechatronics.2004.10.003.

[2] B. Gospodarič, D. Vončina, and B. Bučar, "Active electromagnetic damping of laterally vibrating ferromagnetic cantilever beam," *Mechatronics*, vol. 17, no. 6, pp. 291–298, Jul. 2007, doi: 10.1016/j.mechatronics.2007.04.002.

[3] B. Liu and H. Hu, "Stabilization of linear undamped systems via position and delayed position feedbacks," *J. Sound Vib.*, vol. 312, no. 3, pp. 509–525, May 2008, doi: 10.1016/j.jsv.2007.11.001.

[4] S. N. Mahmoodi and M. Ahmadian, "Active vibration control with modified positive position feedback," *J. Dyn. Syst., Meas., Control*, vol. 131, no. 4, pp. 1–8, Jul. 2009, doi: 10.1115/1.3089565.

[5] R. R. Orszulik and J. Shan, "Vibration control using input shaping and adaptive positive position feedback," *J. Guid., Control, Dyn.*, vol. 34, no. 4, pp. 1031–1044, Jul. 2011, doi: 10.2514/1.52287.

[6] J. Warminski, M. Bochenski, W. Jarzyna, P. Filipek, and M. Augustyniak, "Active suppression of nonlinear composite beam vibrations by selected control algorithms," *Commun. Nonlinear Sci. Numer. Simul.*, vol. 16, no. 5, pp. 2237–2248, May 2011, doi: 10.1016/j.cnsns.2010.04.055.

[7] W. A. El-Ganaini, A. Kandil, M. Eissa, and M. Kamel, "Effects of delayed time active controller on the vibration of a nonlinear magnetic levitation system to multi excitations," *J. Vib. Control*, vol. 22, no. 5, pp. 1257–1275, Mar. 2016, doi: 10.1177/1077546314536753.

[8] A. Kandil and W. A. El-Ganaini, "Investigation of the time delay effect on the control of rotating blade vibrations," *Eur. J. Mech. A, Solids*, vol. 72, pp. 16–40, Nov. 2018, doi: 10.1016/j.euromechsol.2018.03.007.

[9] D. Huang and W. Xu, "Performance characteristics of a real-power viscoelastic isolation system under delayed PPF control and base excitation," *Nonlinear Dyn.*, vol. 88, no. 3, pp. 2035–2050, May 2017, doi: 10.1007/s11071-017-3360-1.

[10] O. A. Garcia-Perez, G. Silva-Navarro, and J. F. Peza-Solis, "Flexible-link robots with combined trajectory tracking and vibration control," *Appl. Math. Model.*, vol. 70, pp. 285–298, Jun. 2019, doi: 10.1016/j.apm.2019.01.035.

[11] E. Bin, J. Shan, M. A. Khushnood, X. Wang, and N. Cui, "Determination of optimal positive position feedback parameters by using nonsmooth H∞ synthesis," *J. Vibrat. Control*, Jul. 2020, Art. no. 107754632094379, doi: 10.1177/1077546320943794.

[12] Y. S. Hamed, A. Kandil, and J. T. Machado, "Utilizing macro fiber composite to control rotating blade vibrations," *Symmetry*, vol. 12, no. 12, p. 1984, Nov. 2020, doi: 10.3390/sym12121984.

[13] J. C. Ji and C. H. Hansen, "Non-linear oscillations of a rotor in active magnetic bearings," *J. Sound Vibrat.*, vol. 240, no. 4, pp. 599–612, Mar. 2001, doi: 10.1006/jsvi.2000.3257.

[14] J. C. Ji, "Stability and Hopf bifurcation of a magnetic bearing system with time delays," *J. Sound Vib.*, vol. 259, no. 4, pp. 845–856, Jan. 2003, doi: 10.1006/jsvi.2002.5125.

[15] W. Zhang and X. P. Zhan, "Periodic and chaotic motions of a rotor-active magnetic bearing with quadratic and cubic terms and time-varying stiffness," *Nonlinear Dyn.*, vol. 41, no. 4, pp. 331–359, Sep. 2005, doi: 10.1007/s11071-005-7959-2.

[16] J. C. Ji, C. H. Hansen, and A. C. Zander, "Nonlinear dynamics of magnetic bearing systems," *J. Intell. Mater. Syst. Struct.*, vol. 19, no. 12, pp. 1471–1491, Dec. 2008, doi: 10.1177/1045389X08088666.

[17] T. Inoue, Y. Sugawara, and M. Sugiyama, "Modeling and nonlinear vibration analysis of a rigid rotor system supported by the magnetic bearing (effects of delays of both electric current and magnetic flux)," *J. Appl. Mech.*, vol. 77, no. 1, pp. 1–10, Jan. 2010, doi: 10.1115/1.3172139.

[18] L. Li, Y. J. Han, and Z. Y. Ren, "Nonlinear study of rotor-AMB system subject to multi-parametric excitations," *Appl. Mech. Mater.*, vols. 397–400, pp. 359–364, Sep. 2013, doi: 10.4028/www.scientific.net/AMM.397-400.359.

[19] X.-D. Yang, H.-Z. An, Y.-J. Qian, W. Zhang, and M.-H. Yao, "Elliptic motions and control of rotors suspending in active magnetic bearings," *J. Comput. Nonlinear Dyn.*, vol. 11, no. 5, pp. 1–8, Sep. 2016, doi: 10.1115/1.4033659.

[20] R. Q. Wu, W. Zhang, and M. H. Yao, "Nonlinear dynamics near resonances of a rotor-active magnetic bearings system with 16-pole legs and time varying stiffness," *Mech. Syst. Signal Process.*, vol. 100, pp. 113–134, Feb. 2018, doi: 10.1016/j.ymssp.2017.07.033.

[21] A. K. Jha and S. S. Dasgupta, "Attenuation of Sommerfeld effect in an internally damped eccentric shaft-disk system via active magnetic bearings," *Meccanica*, vol. 54, nos. 1–2, pp. 311–320, Jan. 2019, doi: 10.1007/s11012-018-00936-7.

[22] Z. Sun, X. Zhang, T. Fan, X. Yan, J. Zhao, L. Zhao, and Z. Shi, "Nonlinear dynamic characteristics analysis of active magnetic bearing system based on cell mapping method with a case study," *Mech. Syst. Signal Process.*, vol. 117, pp. 116–137, Feb. 2019, doi: 10.1016/j.ymssp.2018.07.030.

[23] J. Wang, S. Ma, P. Hao, and H. Yuan, "Hopf bifurcation and control of magnetic bearing system with uncertain parameter," *Complexity*, vol. 2019, pp. 1–12, Dec. 2019, doi: 10.1155/2019/1641953.

[24] X.-Q. Fang, F.-N. Liu, and S.-P. Yang, "Nonlinear dynamic analysis of worn oil-lubricated rolling bearings," *Proc. Inst. Mech. Eng. E, J. Process Mech. Eng.*, vol. 234, no. 2, pp. 214–221, Apr. 2020, doi: 10.1177/0954408920907541.

[25] N. A. Saeed and A. Kandil, "Lateral vibration control and stabilization of the quasiperiodic oscillations for rotor-active magnetic bearings system," *Nonlinear Dyn.*, vol. 98, no. 2, pp. 1191–1218, Oct. 2019, doi: 10.1007/s11071-019-05256-3.

[26] A. Kandil, M. Sayed, and N. A. Saeed, "On the nonlinear dynamics of constant stiffness coefficients 16-pole rotor active magnetic bearings system," *Eur. J. Mech. A, Solids*, vol. 84, Nov. 2020, Art. no. 104051, doi: 10.1016/j.euromechsol.2020.104051.

[27] A. Kandil, "Investigation of the whirling motion and rub/impact occurrence in a 16-pole rotor active magnetic bearings system with constant stiffness," *Nonlinear Dyn.*, vol. 102, no. 4, pp. 2247–2265, Dec. 2020, doi: 10.1007/s11071-020-06071-x.

[28] N. A. Saeed and A. Kandil, "Two different control strategies for 16-pole rotor active magnetic bearings system with constant stiffness coefficients," *Appl. Math. Model.*, vol. 92, pp. 1–22, Apr. 2021, doi: 10.1016/j.apm.2020.11.005.

[29] W. S. Ma, W. Zhang, and Y. F. Zhang, "Stability and multi-pulse jumping chaotic vibrations of a rotor-active magnetic bearing system with 16-pole legs under mechanical-electric-electromagnetic excitations," *Eur. J. Mech. A, Solids*, vol. 85, Jan. 2021, Art. no. 104120, doi: 10.1016/j.euromechsol.2020.104120.

[30] G. Schweitzer and E. H. Maslen, *Magnetic Bearings: Theory, Design, and Application to Rotating Machinery*. Berlin, Germany: Springer, 2009.

[31] A. Nayfeh and D. Mook, *Nonlinear Oscillations*. New York, NY, USA: Wiley, 1995.

[32] A. H. Nayfeh and B. Balachandran, *Applied Nonlinear Dynamics*. New York, NY, USA: Wiley, 1995.

[33] Y. Sun, J. Xu, H. Qiang, W. Wang, and G. Lin, "Hopf bifurcation analysis of maglev vehicle–guideway interaction vibration system and stability control based on fuzzy adaptive theory," *Comput. Ind.*, vol. 108, pp. 197–209, Jun. 2019, doi: 10.1016/j.compind.2019.03.001.

[34] Y. Sun, J. Xu, G. Lin, W. Ji, and L. Wang, "RBF neural network-based supervisor control for maglev vehicles on an elastic track with network time-delay," *IEEE Trans. Ind. Informat.*, early access, Oct. 19, 2020, doi: 10.1109/tii.2020.3032235.

[35] Y. Sun, J. Xu, H. Wu, G. Lin, and S. Mumtaz, "Deep learning based semi-supervised control for vertical security of maglev vehicle with guaranteed bounded airgap," *IEEE Trans. Intell. Transp. Syst.*, early access, Jan. 1, 2021, doi: 10.1109/TITS.2020.3045319.

ALI KANDIL received the M.Sc. and Ph.D. degrees in vibration control of nonlinear dynamical systems from the Faculty of Electronic Engineering, Menoufia University, in 2014 and 2018, respectively. He is currently working at the Faculty of Electronic Engineering, Menoufia University, as an Assistant Professor of engineering mathematics. His current research interests include vibration control, nonlinear dynamics, bifurcation theory, and stability theory.

Y. S. HAMED received the M.Sc. and Ph.D. degrees in mathematics from the Faculty of Science, Menoufia University, Egypt, in 2005 and 2009, respectively. He is currently a Professor of engineering mathematics at the Department of Physics and Engineering Mathematics, Faculty of Electronic Engineering, Menoufia University. He has been a Professor of mathematics at the Department of Mathematics and Statistics, Taif University, Saudi Arabia. He supervised and examined some of the M.Sc. and Ph.D. candidates. His research interests include theory of differential equations and its application, numerical analysis, modeling, dynamical systems control, chaotic systems, renewable energy systems, vibration control and computational methods for solving differential equations, and engineering systems. He is an Editor of *International Journal of Control, Automation and Systems (IJCAS)*.

● ● ●